

UC Davis

UC Davis Previously Published Works

Title

Optimal wind patterns for biological production in shelf ecosystems driven by coastal upwelling

Permalink

<https://escholarship.org/uc/item/1bj3r90g>

Journal

Theoretical Ecology, 3(1)

ISSN

1874-1746

Authors

Yokomizo, Hiroyuki
Botsford, Louis W.
Holland, Matthew D.
[et al.](#)

Publication Date

2010-02-01

DOI

10.1007/s12080-009-0053-5

Peer reviewed

Optimal wind patterns for biological production in shelf ecosystems driven by coastal upwelling

Hiroyuki Yokomizo · Louis W. Botsford ·
Matthew D. Holland · Cathryn A. Lawrence ·
Alan Hastings

Received: 21 October 2008 / Accepted: 3 June 2009 / Published online: 23 June 2009
© The Author(s) 2009. This article is published with open access at Springerlink.com

Abstract Major upwelling systems around the world provide marine productivity and fishery yield out of proportion to their area. Upwelling winds have the counteracting effects that stronger winds upwell more nutrients to the surface for higher production, but they also transport that production off continental shelves where it may not be consumed by shelf-dwelling species. Because the patterns of wind fluctuations vary in these systems, we determined the conditions for maximal biological production using a simple conveyor belt model. The conditions are that: (1) the average cross-shelf velocity produced by the winds be the value that provides the maximum production with constant winds and (2) that the wind pattern be periodic with period

equal to the cross-shelf transport time that results from maximizing production with constant winds. Examination of an example using winds in central California indicated wind patterns optimal for phytoplankton occurred more frequently than those for zooplankton.

Keywords Upwelling · Phytoplankton · Zooplankton · Variable winds · Cross-shelf transport · Mixed layer conveyor model

Introduction

Upwelling ecosystems along the eastern boundaries of major oceans (North and South Pacific and Atlantic) occupy less than 1% of the global ocean area, yet they contribute about 20% of global fish production (Cushing 1971; Mann 2000; Ryther 1969). This inordinate level of productivity is attributed to upwelling, bringing nutrients to the surface from below the depth where there is sufficient light penetration for photosynthesis. Coastal upwelling is caused by strong winds in an equator-ward direction, which cause surface transport in the offshore direction (termed Ekman transport) and consequent flow of cool, nutrient-rich water from depth (i.e., upwelling) to replace water transported away from the shore (e.g., Mann 2000). There is great interest in understanding the high temporal and spatial variability in this productivity (Carr 1998; Carr and Kearns 2003; Thomas et al. 2003) because of its bottom-up influence on the productivity of fisheries at higher trophic levels (e.g., Botsford and Wickham 1975; Nickelson 1986) and the possibility that upwelling strength may respond to increased CO₂ (Bakun 1990; McGregor et al. 2007).

A common approach to understanding the effects of upwelling on higher trophic levels is to examine covari-

H. Yokomizo · M. D. Holland · A. Hastings
Department of Environmental Science and Policy,
University of California,
Davis, CA 95616, USA

H. Yokomizo
CSIRO Sustainable Ecosystems,
306 Carmody Road,
St. Lucia, QLD 4067, Australia

H. Yokomizo (✉)
Research Center for Environmental Risk,
National Institute for Environmental Studies,
Onogawa 16-2,
Tsukuba 305-8506, Japan
e-mail: hiroyuki.yokomizo@nies.go.jp

L. W. Botsford
Department of Wildlife, Fish and Conservation Biology,
University of California,
Davis, CA 95616, USA

C. A. Lawrence
Department of Land, Air, and Water Resources,
University of California,
Davis, CA 95616, USA

ability between biological processes and the volume of water upwelled, as computed from coastal winds (e.g., Bakun 1973). This is typically done by computing correlations between wind strength or an index of volume upwelled and an indicator of productivity such as recruitment, individual growth, population biomass, or fishery catch, either on interannual time scales (e.g., annual recruitment of crabs (Botsford and Wickham 1975) and annual early ocean survival of salmon (Nickelson 1986)) or daily synoptic time scales (e.g., growth rates of rockfish (Hobson and Chess 1988) and barnacles (Sanford and Menge 2001)). The volume upwelled used in interannual comparisons is typically the volume summed or averaged over the local upwelling season. One of the potential problems with these approaches based on upwelled volume is that while higher winds lead to greater upwelled volume, they also lead to more rapid transport of water offshore, possibly beyond the edge of the continental shelf, and any consequent productivity would then be lost to the shelf ecosystem (Botsford et al. 2006). The shelf ecosystem includes many species of fish and invertebrates that occupy continental shelf habitat and contribute to global fisheries. For example, in California, important commercial species of crustaceans, rockfish, flatfish, and other fish are found on the continental shelf (Leet et al. 2001).

Because of this potential for loss of productivity, biological oceanographers are aware of the importance to productivity of the strength of the wind as well as its temporal variability. Periods of strong, upwelling favorable winds are interrupted by frequent (synoptic scale, i.e., daily to weekly) periods of relaxation of upwelling winds. These relaxations are seen to benefit the productivity observed near shore by allowing additional time on the shelf for upwelled nutrients to be converted to primary and secondary production. There is often speculation regarding what the best pattern of winds is (e.g., 1 day of high winds, 4 days of relaxation), but the optimal pattern has not been formally derived (e.g., Carr 1998; Dugdale et al. 2006; Wilkerson et al. 2006).

We formulated a one-dimensional model with cross-shelf transport of upwelled water and off-shelf advective losses to study behavior of upwelling driven production (Botsford et al. 2003, 2006). We fashioned our model after the commonly used idealization of upwelling as a conveyor belt transporting nutrient rich water to the surface, then offshore, while the upwelled water is replaced by an onshore conveyor at the bottom (Fig. 1, e.g., Wilkerson and Dugdale 1987). Our mixed layer conveyer (MLC) model characterizes the development of phytoplankton and zooplankton in each parcel of water after it is upwelled to the surface and is transported across the shelf at velocities determined by standard formulations of Ekman transport. This model includes the essential dynamics of upwelling in

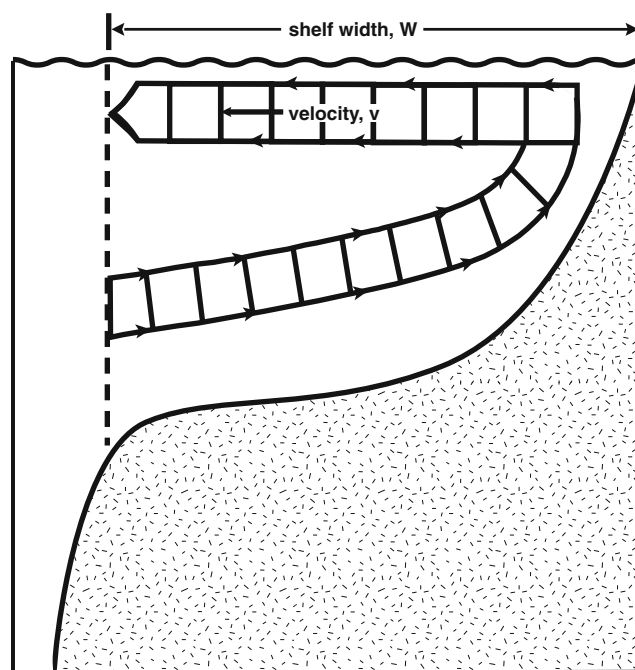


Fig. 1 A schematic of the mixed-layer conveyor concept of biological production from upwelling. Upwelling winds in the direction out of the plane drive surface waters offshore (*to the left*), causing upwelling near shore of nutrient rich waters from below the photic zone. Phytoplankton, then zooplankton populations develop from these nutrients as this water is transported offshore toward the edge of the shelf

the direction across the continental shelf, ignoring along-shore transport (see Botsford et al. (2003, 2006) and Wainwright et al. (2007) for further justification of this step). It is a compromise between two- and three-dimensional primitive equation, circulation models (e.g., Gruber et al. 2006; Spitz et al. 2003) and simple “box” models with no spatial dimension, in which upwelling is represented by adding water with high nutrients, no phytoplankton and no zooplankton to the model state (e.g., Carr 1998; Hofmann and Ambler 1988; Olivieri and Chavez 2000; Peña 1994). It lends itself more easily to analysis and extensive computation than the primitive equation model, yet retains the essential cross-shelf spatial dynamics that are of primary interest here. Wainwright et al. (2007) used the same conveyor belt approach to compare two nitrogen-phytoplankton-zooplankton (NPZ) models to plankton data off the Oregon coast.

We have used this model to characterize the dependence of various types of biological production on the magnitude of constant winds (Botsford et al. 2003) and to describe the response of production to time-varying winds on various time scales (Botsford et al. 2006). Here, we describe another approach to understanding the relationship between wind variability and biological productivity, asking the question, what temporal pattern leads to the highest new

production? This question was raised by the empirical analysis of the responses of the MLC model to historical wind series in Botsford et al. (2006; i.e., Fig. 2a) but was also inspired by discussions with biological oceanographic

colleagues regarding the best wind patterns (e.g., 2 days of upwelling, 1 day of relaxation, etc., see “Discussion” in Wilkerson et al. 2006) and previous analyses by Carr (1998).

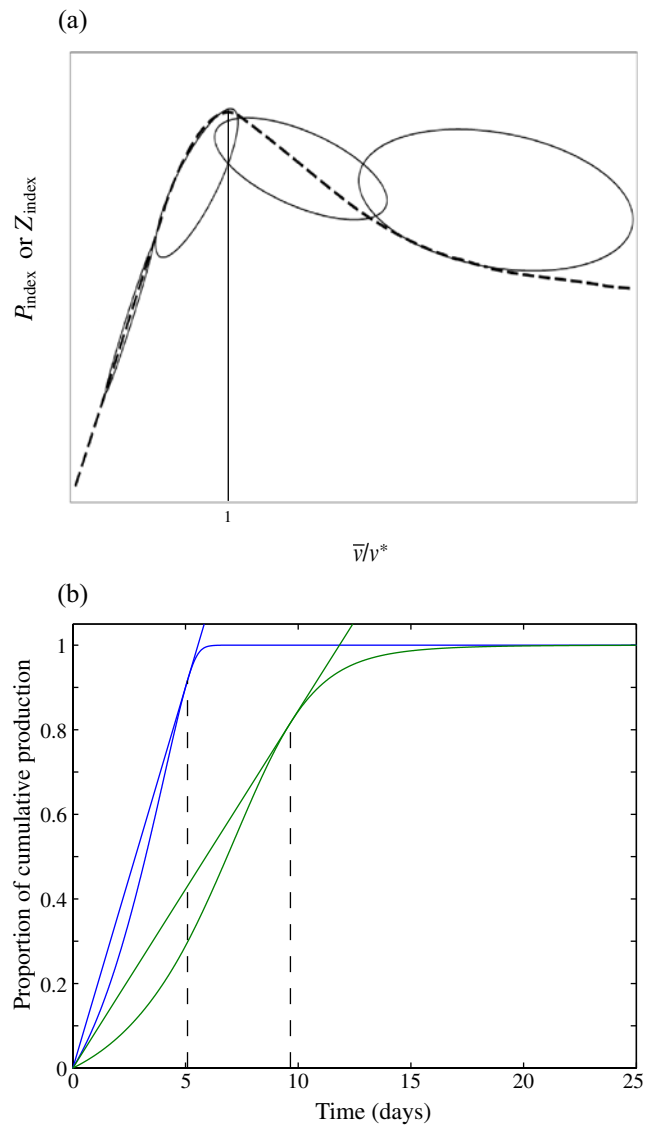


Fig. 2 Static and dynamic responses of the MLC model for upwelling production. The *dashed curve* in **a** is the response of new production to different values of constant winds, hence, constant cross-shelf velocity (Botsford et al. 2003). The values of P_{index} or Z_{index} would depend on local maximum concentrations possible by complete uptake of nutrients. The cross-shelf velocities are normalized by v^* , the ratio of the local shelf width W to T^* . The *ellipses* would enclose values of annual productivity resulting from different patterns of time-varying winds and consequent time-varying velocities. Different *ellipses* correspond to different shelf widths (or development rates of phytoplankton or zooplankton). The shelf width (development rate) changes from *very wide* (fast) on the *left* to *narrow* (slow) on the *right* (see Botsford et al. 2006 for details). The variable \bar{v} is the mean annual value of the cross-shelf velocity; **b** is the temporal response of the NPZ model in Eqs. 1–3b, with a tangent line that defines the cross-shelf transit time (T^*) that maximizes productivity for constant wind (Botsford et al. 2003)

The model

In the MLC model (Botsford et al. 2003, 2006), the rate of shelf production for phytoplankton and zooplankton is the product of the velocity at which parcels are brought to the surface and advected offshore and the cumulative uptake per parcel up to the time that it leaves the shelf. Biological material transported off the shelf is considered lost to the shelf ecosystem. Rate of production at time t is represented by

$$B(t) = v(t)F[T(t)], \tag{1}$$

where $v(t)$ = cross-shelf velocity, $F[s]$ = cumulative production after time s at the surface and $T(t)$ = shelf transit time for a particle upwelled at time t .

The cross-shelf velocity is determined from the wind using relationships describing Ekman transport in upwelling systems (Botsford et al. 2006). Cumulative production of zooplankton and phytoplankton are determined from a simple ecosystem model for nutrients, N , phytoplankton, P , and zooplankton, Z :

$$\frac{dN}{dt} = -\frac{V_m N}{K_s + N} f(I)P, \tag{2a}$$

$$\frac{dP}{dt} = \frac{V_m N}{K_s + N} f(I)P - mP - R_m(1 - e^{-AP})Z, \tag{2b}$$

$$\frac{dZ}{dt} = \gamma R_m(1 - e^{-AP})Z - gZ, \tag{2c}$$

where $f(I)$ is the dependence of phytoplankton growth of mean light level I , obtained by averaging light over the mixed layer, accounting for shading by the phytoplankton (see Botsford et al. (2006) for details) and the definition of variables is in Table 1. This is the model of Franks and Walstad (1997) modified to represent new production only (Dugdale and Goering 1967) by removing the inherent instability in the close coupling of regenerated production. Other approaches to removing this instability include adding a parabolic mortality rate and adding time delays or diffusion (e.g., Botsford et al. 2003; Edwards et al. 2000; Newberger et al. 2003; Steele and Henderson 1992). The model was parameterized to produce the rates of increase and levels of productivity observed in the Wind Events and Shelf Transport (WEST) experiment (Table 1; Largier et al. 2006; Wilkerson et al. 2006). Parameter values will vary

Table 1 Symbol descriptions, parameter values, and units for the NPZ model

Symbol	Symbol description	Value	Units
I	Average irradiance	440 (surface)	$\mu\text{Em}^{-2} \text{ s}^{-1}$
K_s	Half saturation for P uptake of N	1.0	$\mu\text{M N}$
N	Nutrient state variable	$N_0=17.5$	$\mu\text{M N}$
P	Phytoplankton state variable	$P_0=2.25$	$\mu\text{M N}$
R_m	Maximum ingestion rate of P by Z	0.6	$\mu\text{M N day}^{-1}$
V_m	Maximum uptake rate of N by P	1.0	$\mu\text{M N day}^{-1}$
Z	Zooplankton state variable	$Z_0=1.5$	$\mu\text{M N}$
g	Natural mortality rate of Z	0.2	day^{-1}
m	Natural mortality rate of P	0.1	day^{-1}
λ	Grazing efficiency of Z on P	0.2	$(\mu\text{M N})^{-1}$
γ	Assimilated fraction of P ingested by Z	0.7	Proportion

with the location of interest in different upwelling systems of the world.

The cumulative uptake of nutrients by phytoplankton, F_P , and the cumulative consumption of phytoplankton by zooplankton, F_Z , were taken to represent the total amount of phytoplankton and zooplankton, respectively, made available to the ecosystem (as in Botsford et al. 2003, 2006). These were expressed as:

$$F_P(T) = \int_0^T \frac{V_m N}{K_s + N} f(I) P dt, \quad (3a)$$

$$F_Z(T) = \int_0^T R_m (1 - e^{-\lambda P}) Z dt. \quad (3b)$$

These depend on the initial nutrient and phytoplankton concentrations and light level (Table 1; see Botsford et al. (2006) for further details). Because the nature of the food chain at higher trophic levels varies greatly with year and location, we did not attempt to model those levels explicitly. Their effects are represented simply as part of the mortality depicted in the term, $-gZ$, in Eq. 2c. Also, note that most species at higher trophic levels possess sufficient motility not to be influenced by offshore transport due to upwelling.

Previous results

Because the results regarding optimal winds depend on our previous results with this model, we review them here briefly. We have characterized the dome-shaped response of this model to constant winds (Botsford et al. 2003; dashed curve in Fig. 2a). Production increases with wind strength at low winds, in proportion to upwelled volume, but

eventually begins to decrease as losses increase off the shelf. The wind velocity that produces maximum production can be determined by graphically obtaining the optimal cross-shelf transit time, T^* , as the time at which a line through the origin is tangent to a plot of cumulative production of either phytoplankton or zooplankton. From Fig. 2b, for the parameter values used here, the optimal constant wind for phytoplankton production is the one that produces a cross-shelf transit time of $T^*=5.09$ days, and the optimal transit time for zooplankton production is $T^*=9.66$ days. The optimal cross-shelf velocity is then $v^*=W/T^*$, where W is the shelf width. In Fig. 2a, velocity is normalized by v^* to obtain a general curve independent of the local pattern of phytoplankton and zooplankton development and local shelf width (see Botsford et al. (2006) for details).

The response of this model to time-varying winds was more complex and depended on timescale (Botsford et al. 2006). We compared the MLC model, which accounts for offshore losses due to high winds, with the conventional volume upwelled. At synoptic timescales, volume upwelled was a reasonably good predictor of shelf productivity. However, that was primarily due to the common effect of relaxation periods (i.e., common periods of zero) in both the volume upwelled and productivity time series rather than volume upwelled accurately representing the productivity calculated from the MLC model. On annual time scales, however, the predictions of volume upwelled and the MLC model driven by constant winds at the mean level, both differed from the annual production calculated from the MLC model with variable winds. Annual total volume upwelled and the annual productivity from the MLC model predicted similar annual productivity for wide shelves and low wind velocities only (Botsford et al. 2006; values of annual productivity for 20 years of real winds would lie within the initial narrow ellipse on the left of Fig. 2a). As assumed mean wind speed increased further (or if assumed shelf width was less or plankton response was slower),

production from the MLC model (represented as the next ellipse to the right in Fig. 2a) became less than predicted by volume upwelled and even less than the constant wind prediction of the MLC model. With further increase in mean wind speed (or lower shelf width or slower plankton response), productivity from the MLC model became greater than the constant wind MLC result (following the sequence of oval shapes moving to the right in Fig. 2a, each of which represents the range that would be seen for a single combination of shelf width, plankton response time, and mean wind velocity). Note that at any specific location, zooplankton would lie in an ellipse to the right of phytoplankton ellipse because the response time is greater.

Results

Optimal cross-shelf velocity pattern

Given this model of the shelf ecosystem, we are interested in the cross-shelf velocity pattern that maximizes upwelling productivity. The velocity pattern that maximizes average $B(t)$ can be any pattern that satisfies two conditions (see Appendix):

$$v(t) = v(t + T^*), \quad (4a)$$

$$\int_t^{t+T^*} v(t) dt = W. \quad (4b)$$

Thus, shelf productivity is maximized by any pattern of cross-shelf velocity that: (1) is periodic with period T^* , the optimal value of cross-shelf transit time for the case with constant wind (and therefore constant cross-shelf velocity), and (2) has a mean velocity equal to the equal to the optimal cross-shelf velocity for the case with constant wind (i.e., W/T^*).

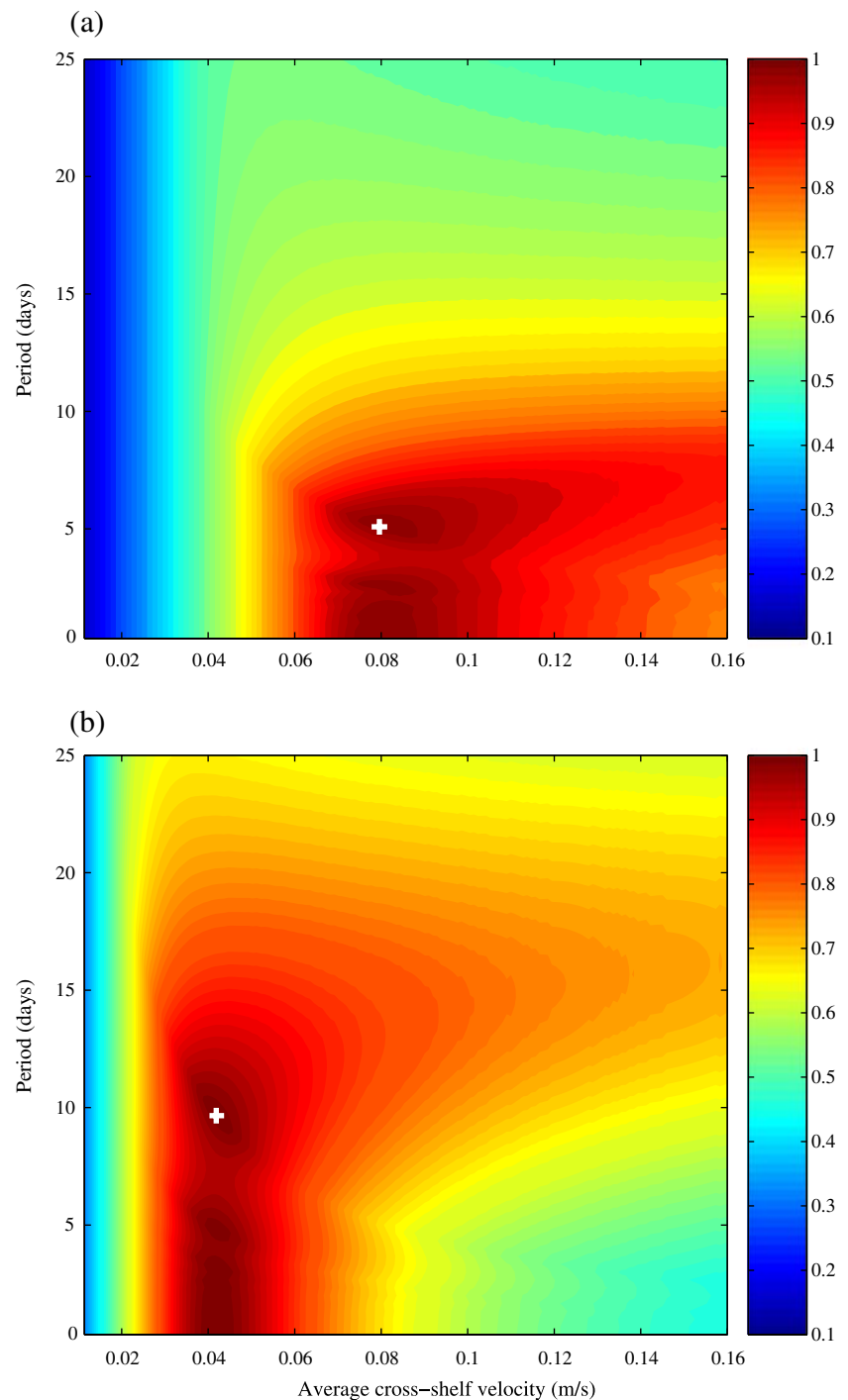
To explore the sensitivity of this result to average cross-shelf velocity and period, we simulated the response of production of phytoplankton and zooplankton to synthetic winds which are at zero wind stress for half the period and twice the mean wind stress for the other half, averaging obviously to the mean velocity. We used the parameter values appropriate for the central California coast (Table 1). The results indicate a maximum of production at the conditions predicted by Eqs. (4a) and (4b), with high values along a ridge toward shorter periods (Fig. 3). The ridge has obvious minor peaks at one half and one fourth of the optimal period, as expected on the basis of these fractions also being periodic with the optimal period. Production is relatively insensitive to the exact value of

higher velocity at the optimal period and the exact value of higher periods at the optimal velocity. For both zooplankton and phytoplankton, production is near optimal over a range of values. Taking phytoplankton as an example, while the optimum is at a period of 5.09 days and a cross-shelf velocity of .08 m/s, series of cross-shelf velocity with a period less than 7.5 days and a mean velocity within $\pm 20\%$ of the optimum mean velocity will yield production that is greater than 90% of the optimum. Also, for periods between 4 and 7 days, greater mean velocities produce near-optimal results. The plots for phytoplankton production (Fig. 3a) and zooplankton production (Fig. 3b) are qualitatively the same, differing only in timescale.

To illustrate how these optimal patterns might occur in real-time series, we plotted an example from the year 2001 of the cross-shelf velocity near Bodega Bay, CA (the site of the WEST experiment), calculated from local buoy winds next to a plot of possible optimal patterns of cross-shelf velocity (Fig. 4a–c). This figure also includes the production that results from each parcel of water upwelled plotted versus time upwelled (Fig. 4d) and the volume upwelled along with the portion of the nutrients in that volume that are converted to phytoplankton and zooplankton (Fig. 4e). From Eqs. 4a and 4b, the optimal patterns must be periodic with a specific period and mean, but the specific pattern is not specified beyond that. For both phytoplankton and zooplankton, we examined wind patterns in which cross-shelf velocities were nonzero over 20%, 40%, 60%, 80%, and 100% of the period T^* and adjusted the nonzero values of cross-shelf velocity so that the mean over T^* was 0.08 m/s (phytoplankton optimum) or 0.042 m/s (zooplankton optimum). Since T^* for phytoplankton is approximately an integer value (5 days), this represented the following patterns of days with a specified wind and days without winds: 1 day on and 4 days off, 2 days on and 3 days off, 3 days on and 2 days off, 4 days on and 1 day off, respectively.

From Fig. 4a and c, taking phytoplankton as an example, one can see that possible optimal patterns are limited by the maximum local wind strength. For example, near Bodega Bay, cross-shelf velocities are never high enough for there to be a 1-day-on-and-4-days-off pattern. However, velocities are high enough for 2-days-on-and-3-days-off patterns to occur. For example, qualitative observations indicate that velocities are near the required value on May 3rd and May 4th followed by 1 day of relaxation, May 10th followed by 3 days of upwelling and May 18th and May 19th followed by 3 days of upwelling. All three of these periods lead to high phytoplankton production, with some times of complete conversion of all nutrients to phytoplankton (Fig. 4e). The pattern closest to the optimal pattern, May 18th and May 19th followed by 3 days of relaxation, is the most productive. Note that while optimal patterns (Fig. 4a, b)

Fig. 3 Time averaged productivity produced by periodic cross-shelf velocities shifting between zero and a constant value, with equal time spent at each, over a range of periods and mean velocities, for phytoplankton (a) and zooplankton (b). The *plus sign* indicates the optimal values indicated by **a** for a shelf width of 35 km, the local shelf with for Bodega Bay

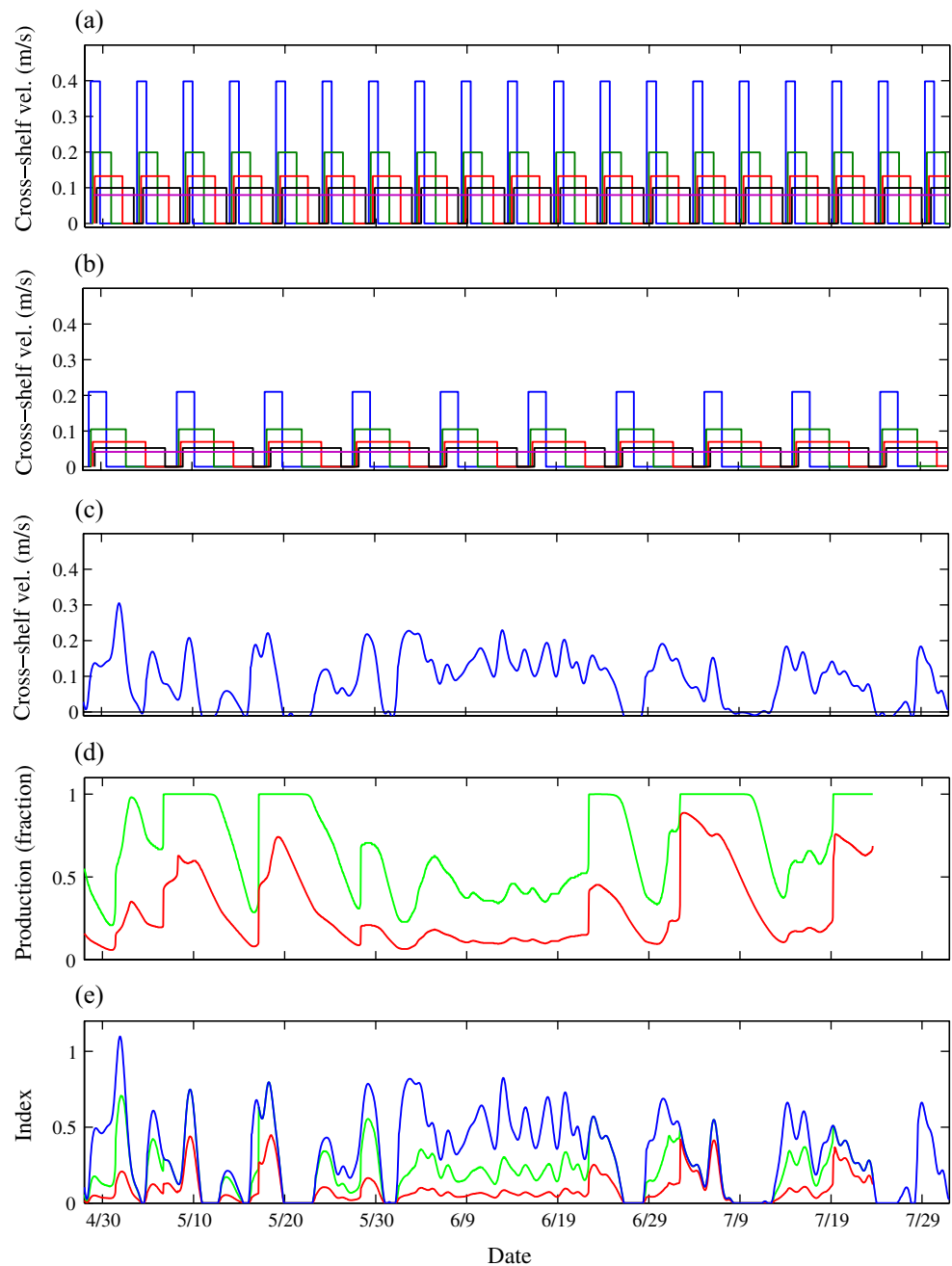


are present in the actual time series (Fig. 4c), they are not immediately repeated; rather, they are separated by periods with other suboptimal patterns.

Following a similar procedure for zooplankton reveals that optimal wind patterns for zooplankton production seldom occur. This is consistent with the fact that in Fig. 4e, nutrients upwelled (the blue line) are seldom completely converted to zooplankton (i.e., the red line is

typically far below the blue line). An exception occurs in the cross-shelf velocities just prior to July 9th (Fig. 4c), where a pattern matching 20% on followed by 80% off (Fig. 4b) occurs, and zooplankton production (Fig. 4e) almost reaches the full potential. That there is seldom an optimal pattern for zooplankton productivity may not be as important as it seems because zooplankton may avoid being passively transported off the shelf (see “Discussion”).

Fig. 4 Comparison of optimal cross-shelf velocity patterns with cross-shelf velocities calculated from buoy winds and calculated production. **a, b** Examples of optimal patterns of cross-shelf velocities for phytoplankton and zooplankton, respectively. *Purple* represents constant wind, *blue* represents 20% on and 80% off, *green* represents 40% on and 60% off, *red* represents 60% on and 40% off, and *black* represents 80% on and 20% off. **c** Actual cross-shelf velocity plotted versus date in 2001 (Botsford et al. 2006). **d** The fraction of maximum possible phytoplankton (*green*) and zooplankton (*red*) production in upwelled parcels, plotted versus the time the parcel was upwelled. The maximum possible in each case corresponds to complete uptake of nutrients. **e** Indices of the volume upwelled at each time (*blue*) and the amount of nutrients in that volume that is converted to phytoplankton (*green*) and zooplankton (*red*). When maximum uptake of phytoplankton or zooplankton has been reached, the *green* or *red* line, respectively, will lie beneath the *blue* line



Discussion

The results obtained here contribute to the ongoing development of an understanding of how temporal variability in upwelling winds leads to high levels of production. They indicate which patterns of winds could produce the maximal cumulative production and the frequency at which they must occur. In addition, they indicate the variables that are important in setting the optimal patterns. Globally, the basic timescale of optimal winds, T^* , is set by the biology, the patterns of cumulative increase in local phytoplankton and zooplankton (e.g., Fig. 2a). The optimal cross-shelf velocity

for shelf production is then set by the shelf width W at that location. The wind pattern is then determined by the relationship between wind and velocity of Ekman transport, which depends on latitude. These results will be useful in studies that collect and compare the characteristics of upwelling systems at various locations (e.g., Carr 1998; Carr and Kearns 2003). In such comparisons, the approach applied here can be followed, but the appropriate parameters, initial conditions, and form of the NPZ model need not be the same. Once formulated for local plankton dynamics, the NPZ model could be run to create plots such as those in Fig. 2b to determine T^* , the period of the optimal velocity

cycles, then local shelf width could be used to set the mean velocity (Eqs. 4a, 4b). The wind speeds associated with a specific cross-shelf velocity would vary with latitude because the relationship involves the Coriolis parameter.

Previous efforts to determine optimal winds have been based on empirical observations of chlorophyll concentration at a specific location and qualitative identification of the patterns leading to the highest value (e.g., Wilkerson et al. 2006). Here, we cast this problem formally as the temporal pattern of the winds leading to the maximum cumulative production by the time the upwelled parcel reaches a specific point, the shelf edge. These two approaches seek very similar goals since the time of maximum observed chlorophyll concentration will be close to the time of maximum cumulative uptake; however, the spatial scales could differ since the moorings from which observations are made are often on the continental shelf, whereas our point at which production was maximized was the shelf edge.

The major new finding here not obtained explicitly from the conventional empirical approach is that there is no single optimal pattern such as m days on, n days off. Optimal relaxation can be of any duration less than the optimal cross-shelf transit time as long as the upwelling winds during the remainder of the optimal period are such that they upwell enough nutrients to produce the optimal value.

In a recent empirical evaluation of the optimal wind pattern at the same locations as the winds in Fig. 4c, Wilkerson et al. (2006) concluded that an optimal window of 3–7 days of relaxed winds following an upwelling pulse was required for chlorophyll accumulation at a mooring located on the shelf. The results presented here differ in that a range of temporal patterns can be optimal and the duration of the relaxation period would depend on the strength of the upwelling pulse. If one assumes that an upwelling pulse lasted 2 days and the cross-shelf velocity was 0.2 m/s and that Wilkerson et al. (2006) were just seeking single patterns with high chlorophyll levels and not the highest levels per unit time produced by repeating patterns, then the results are quite similar. Since they put no premium on having the production cycle be shorter so that it could be repeated more times, they allowed the optimal relaxation period to last over a duration greater than 3 days. However, if we account for the fact that the mooring location was at a shorter distance from the shore than the shelf edge, even shorter timescales would be predicted to be optimal.

The differences between optimal patterns for phytoplankton and zooplankton production (Fig. 4a, b) raise the question of which we should pay attention to in trying to gauge bottom–up influences on general levels of production at higher trophic levels. To phrase this another way, why concern ourselves with optimal wind patterns for phytoplankton production if we are ultimately concerned with production

of zooplankton and higher trophic levels? The distinction that determines the importance of optimal wind patterns is the degree of susceptibility to the influence of offshore advection. In the extreme, we do not include fish in our analysis because they are strong swimmers, hence, not susceptible to offshore advection due to upwelling (and further, may not be near the surface, at risk of export off the shelf). Some species of zooplankton may be ignored for similar reasons. Analyses of zooplankton data in the WEST project indicated that local krill (*Euphausia pacifica*) may employ vertical migration to move between the offshore upwelling flow near the surface and the onshore flow near the bottom to maintain their position on the shelf and avoid transport offshore (Dorman et al. 2005). Similarly, off Oregon, later stages of both euphausiids and copepods were found deeper than early stages, which were in the upper layer (Lamb and Peterson 2005). These indications that zooplankton may not be susceptible to loss off of the shelf suggest that we should focus on the optimal wind pattern for phytoplankton as a general determinant of upwelling production.

This work is similar in intent to other efforts to determine the response of marine primary and secondary production to periodic wind forcing. For example, Carr (1998) compared the response of a nonspatial NPZ model representing new production (i.e., one autotroph and one heterotroph, similar to our model) to a similar model with additional productive pathways (i.e., three autotrophs and four heterotrophs). The upwelling forcing used a variety of pulse amplitudes, durations, and periodic spacing from several locations based on local satellite scatterometer winds. However, her results would not be directly comparable to ours since the effect of upwelling was to periodically change the concentrations in her nonspatial model by adding upwelled water. Thus, the mechanism in her model was one of resetting the sequence of “succession” from nutrients to phytoplankton to zooplankton, in a nonspatial model, rather than one that involves losing productivity off the shelf during periods of high upwelling winds, as assessed here. On the other hand, she raises the question of the wind frequencies that will produce maximal productivity. Our results suggest that optimal wind would have a strong component near frequencies of $1/T^*$, indicating the timescale of the wind required for high production depends solely on the biology.

Our results must be weighed in the light of the fact that they were reached using a highly idealized model that only approximates the complex three-dimensional circulation. Viewing the three-dimensional circulation patterns in coastal upwelling systems as a single conveyor belt is a crude approximation. However, it has a long history as an intuitive, canonical model (Wilkerson and Dugdale 1987; Kudela et al. 2008) and even as a way of designing empirical studies that follow upwelled parcels along a

plume of upwelled water (e.g., MacIsaac et al. 1985). Many other aspects of biological productivity in upwelling systems vary with location, such as biological parameters of NPZ models, micronutrient limitation, and nutrient content of source waters. These can be accounted for in the formulation of the NPZ model for each location. Our results provide simple rules that can be used to compare upwelling systems at different times and locations and that can be compared to results from more realistic circulation models where they are available.

Acknowledgements We thank NSF Coastal Ocean Processes Program funded by OCE-9910897 and a Grant-in-Aid for Scientific Research of Japan Society for the Promotion of Science to HY for support. We are also grateful to the following people for their helpful comments: R. Dugdale, N. Huth, A. Richardson, K. Ridgway, and R. Schlicht.

Open Access This article is distributed under the terms of the Creative Commons Attribution Noncommercial License which permits any noncommercial use, distribution, and reproduction in any medium, provided the original author(s) and source are credited.

Appendix

Derivation of optimal wind pattern

The rate of production at time t is given by

$$B(t) = v(t)F[T(t)].$$

The total production in a period of time from 0 to τ is therefore obtained by integrating $B(t)$ over the time interval $0 \leq t \leq \tau$

$$\int_0^\tau B(t)dt = \int_0^\tau v(t)F[T(t)]dt,$$

and the average production rate in this time interval is represented by

$$\frac{1}{\tau} \int_0^\tau B(t)dt.$$

Proposition Assume that the expression $\frac{F(t)}{t}$ obtains an isolated global maximum at the value T^* . Let $\varepsilon > 0$ be any positive number. Then, among all cross-shelf wind patterns v which satisfy $v(t) \geq \varepsilon$ for all t , the long-term average production

$$\lim_{t \rightarrow \infty} \frac{1}{\tau} \int_0^\tau B(t)dt$$

is maximal if and only if $T(t) = T^*$ for all t .

Proof. First, we define $V(t) = \int_0^t v(s)ds$, which represents the total distance the stream of particles has moved since time 0, or equivalently, the position at time t of the particle that was upwelled at time 0. Due to the assumption $v(t) \geq \varepsilon$, V is a strictly increasing function; hence, it is possible to calculate the inverse V^{-1} .

Using the substitution $x = V(t)$, we can express the total production $\alpha(\tau)$ in the interval $0 \leq t \leq \tau$ in terms of an integral over space:

$$\begin{aligned} \alpha(\tau) &= \int_0^\tau v(t)F[T(t)]dt \\ &= \int_0^\tau \frac{dV(t)}{dt} F[T(V^{-1}(V(t)))]dt \\ &= \int_0^{V(\tau)} F[T(V^{-1}(x))]dx. \end{aligned}$$

Let $g(x)$ be the average production rate per time unit of the particle that entered the shelf at time t :

$$g(x) = \frac{F[T(V^{-1}(x))]}{T(V^{-1}(x))}.$$

Since $T(V^{-1}(x)) = V^{-1}(x + W) - V^{-1}(x)$, the integral above can be written as follows:

$$\begin{aligned} \alpha(\tau) &= \int_0^{V(\tau)} (V^{-1}(x + W) - V^{-1}(x))g(x)dx \\ &= \int_0^{V(\tau)} \left\{ \int_{V^{-1}(x)}^{V^{-1}(x+W)} g(x)dt \right\} dx \\ &= \int_A g(x)d(x, t), \end{aligned}$$

where $A = \{(x, t) | 0 \leq x \leq V(\tau), x \leq V(t) \leq x + W\}$. We will show that for the long-term average, the set A can be replaced with the set

$$C = \{(x, t) | 0 \leq V(t) \leq V(\tau), V(t) - W \leq x \leq V(t)\}.$$

Let $\gamma(\tau) = \int_C g(x)d(x, t)$. Since we would like to neglect boundary conditions (initial condition and end condition), we consider the long-term average. Then, the error we

make in the long-term average when using $\gamma(\tau)$ instead of $\alpha(\tau)$ is

$$\delta = \left| \lim_{\tau \rightarrow \infty} \frac{1}{\tau} \gamma(\tau) - \lim_{\tau \rightarrow \infty} \frac{1}{\tau} \alpha(\tau) \right|$$

$$\leq \lim_{\tau \rightarrow \infty} \frac{1}{\tau} \int_{(A \setminus C) \cup (C \setminus A)} |g(x)| d(x, t).$$

We calculate upper bounds for the area covered by the sets $A \setminus C$ and $C \setminus A$ in the two-dimensional (x, t) plane. Elements $(x, t) \in C \setminus A$ have the property $0 \leq V(t) \leq x + W$ and $x \leq V(\tau)$ because they are in C , but $x < 0$ because they are not in A , hence $-W \leq x < 0$ and $0 \leq t < V^{-1}(W)$. The area of $C \setminus A$ is, therefore, bounded by $W(V^{-1}(W) - 0) = WT(0)$. Similarly, elements $(x, t) \in A \setminus C$ satisfy $x \leq V(\tau)$ and $0 \leq V(t) \leq x + W$ because they are in A , but $V(\tau) < V(t)$ because they are not in C . Hence, $V(\tau) - W < x \leq V(\tau)$ and $\tau < t \leq V^{-1}(V(\tau) + W)$ and the area of $A \setminus C$ is bounded by $W(V^{-1}(V(\tau) + W) - \tau) = WT(\tau)$. Since g is bounded by $g(T^*)$ according to the definition of T^* , we obtain

$$\delta \leq \lim_{\tau \rightarrow \infty} \frac{1}{\tau} (WT(0) + WT(\tau))g(T^*) = 0.$$

Hence, we can consider $\gamma(\tau)$ instead of $\alpha(\tau)$ for the optimization of the wind pattern. We have

$$\gamma(\tau) = \int_0^\tau \left\{ \int_{V(t)-W}^{V(t)} g(x) dx \right\} dt$$

$$= \int_0^\tau \left\{ \int_0^W g(y + V(t) - W) dy \right\} dt.$$

The upper and lower limits in the last integral are independent of the wind pattern. Thus, for τ approaching infinity, the integral is maximal if and only if g is such that it has the maximum value $g(T^*)$ everywhere, which is equivalent to the condition $T(t) = T^*$ for all t . Although we assumed $v(t) \geq \varepsilon$, the error should be negligible even when $v(t) = 0$

References

- Bakun A (1973) Coastal upwelling indices, west coast of North America, 1946–1971. NOAA, Washington, D.C. Tech Rep NMFS SSRF-671, 103 pp
- Bakun A (1990) Global climate change and intensification of coastal ocean upwelling. *Science* 247:198–201
- Botsford LW, Wickham DE (1975) Correlation of upwelling index and Dungeness crab catch. *Fish Bull* 73:901–907
- Botsford LW, Lawrence CA, Dever EP, Hastings A, Largier J (2003) Wind strength and biological productivity in upwelling systems: an idealized study. *Fish Oceanogr* 12:245–259
- Botsford LW, Lawrence CA, Dever EP, Hastings A, Largier J (2006) Effects of variable winds on biological productivity on continental shelves in coastal upwelling systems. *Deep-sea Res 2, Top Stud Oceanogr* 53:3116–3140
- Carr M-E (1998) A numerical study of the effect of periodic nutrient supply on pathways of carbon in a coastal upwelling regime. *J Plankton Res* 20:491–516
- Carr M-E, Kearns EJ (2003) Production regimes in four Eastern Boundary Current systems. *Deep-sea Res 2, Top Stud Oceanogr* 50:3199–3221
- Cushing DH (1971) Upwelling and the production of fish. *Adv Mar Biol* 9:255–334
- Dugdale RC, Goering JJ (1967) Uptake of new and regenerated forms of nitrogen in primary productivity. *Limnol Oceanogr* 12:196–206
- Dugdale RC, Wilkerson FP, Hogue VE, Marchi A (2006) Nutrient controls on new production in the Bodega Bay, California, coastal upwelling plume. *Deep-sea Res 2, Top Stud Oceanogr* 53:3049–3062
- Dorman J, Bollens S, Slaughter A (2005) Population biology of euphausiids off northern California and effects of short time-scale wind events on *Euphausia pacifica*. *Mar Ecol Prog Ser* 288:183–198
- Edwards CA, Powell TA, Batchelder HP (2000) The stability of an NPZ model subject to realistic levels of vertical mixing. *J Mar Res* 58:37–60
- Franks PJS, Walstad LJ (1997) Phytoplankton patches at fronts: a model of formation and response to wind events. *J Mar Res* 55:1–29
- Gruber N, Frenzel H, Doney SC, Marchesiello P, McWilliams JC, Moisan JR, Oram JJ, Plattner G-K, Solzenbach KD (2006) Eddy-resolving simulation of plankton ecosystem dynamics in the California Current System. *Deep-sea Res 1, Oceanogr Res Pap* 53:1483–1516
- Hobson ES, Chess JR (1988) Trophic relations of the blue rockfish, *Sebastes mytinus*, in a coastal upwelling system off northern California. *Fish Bull* 86:715–743
- Hofmann EE, Ambler JW (1988) Plankton dynamics on the outer southeastern U.S. continental shelf. Part II: a time-dependent biological model. *J Mar Res* 46:883–917
- Kudela RM, Banas NS, Barth JA, Frame ER, Jay DA, Largier JL, Lessard EJ, Peterson TD, Vander Woude AJ (2008) New insights into the controls and mechanisms of plankton productivity in coastal upwelling waters of the northern California Current system. *Oceanogr* 21:46–59
- Lamb J, Peterson W (2005) Ecological zonation of zooplankton in the COAST study region off Oregon in June and August of 2001, with consideration of retention mechanisms. *J Geophys Res* 110: C10S15. doi:10.1029/2004JC002520
- Largier JL, Lawrence CA, Roughan M, Kaplan DM, Dever EP, Dorman CE, Kudela RM, Bollens SM, Wilkerson FP, Dugdale RC, Botsford LW, Garfield N, Kuebel-Cervantes B, Koracin D (2006) WEST: a northern California study of the role of wind-driven transport in the productivity of coastal plankton communities. *Deep-sea Res 2, Top Stud Oceanogr* 53:2833–2849
- Leet WS, Dewees CM, Klingbeil R, Larson EJ (2001) California's living marine resources: a status report. California Department of Fish and Game, Sacramento 592 pp
- MacIsaac JJ, Dugdale RC, Barber RT, Blasco D, Packard TT (1985) Primary production cycle in an upwelling center. *Deep-sea Res 1, Oceanogr Res Pap* 32:503–529
- Mann KH (2000) Ecology of coastal waters, with implications for management, 2nd edn. Blackwell Science, Boston, p 406
- McGregor HV, Dima M, Fischer HW, Mulitza S (2007) Rapid 20th-century increase in coastal upwelling off northwest Africa. *Science* 315:637–639
- Newberger PA, Allen JS, Spitz YH (2003) Analysis and comparison of three ecosystem models. *J Geophys Res* 108:6.1–6.21. doi:10.1029/2001JC001182

- Nickelson TE (1986) Influences of upwelling, ocean temperature and smolt abundance on marine survival of coho salmon (*Oncorhynchus kisutch*) in Oregon production area. *Can J Fish Aquat Sci* 43:527–535
- Olivieri RA, Chavez FP (2000) A model of plankton dynamics for the coastal upwelling system of Monterey Bay, California. *Deep-sea Res 2, Top Stud Oceanogr* 47:1077–1106
- Peña MA (1994) New production in the tropical Pacific region. PhD Thesis, Dalhousie University
- Ryther JH (1969) Photosynthesis and fish production in the sea. *Science* 166:72–80
- Sanford E, Menge BA (2001) Spatial and temporal variation in barnacle growth in a coastal upwelling system. *Mar Ecol Prog Ser* 201:143–157
- Spitz YH, Newberger PA, Allen JS (2003) Ecosystem response to upwelling off the Oregon coast: behavior of three nitrogen-based models. *J Geophys Res* 108:7.1–7.22. doi:[10.1029/2001JC001181](https://doi.org/10.1029/2001JC001181)
- Steele JH, Henderson EW (1992) The role of predation in plankton models. *J Plankton Res* 14:157–172
- Thomas A, Strub PT, Carr ME, Weatherbee R (2003) Comparisons of chlorophyll variability between the four major global eastern boundary currents. *Int J Remote Sens* 25:1443–1447
- Wainwright TC, Feinberg LR, Hooff RC, Peterson WT (2007) A comparison of two lower trophic models for the California Current System. *Ecol Model* 202:120–131
- Wilkerson FP, Dugdale RC (1987) The use of large ship-board barrels and drifters to study the effects of coastal upwelling on phytoplankton dynamics. *Limnol Oceanogr* 32:368–382
- Wilkerson FP, Lassiter AM, Dugdale RC, Marchi A, Hogue VE (2006) The phytoplankton bloom response to wind events and upwelled nutrients during the CoOP-WEST Study. *Deep-sea Res 2, Top Stud Oceanogr* 53:3023–3048